Bone Morphology and Mechanical Properties in Murine Models of Chronic Kidney Disease

by

Andrew C Cureton

B.A., Bethel University, 2008

B.S., Messiah College, 2009

A thesis submitted to the

Faculty of the Graduate School of the

University of Colorado in partial fulfillment

of the requirements for the degree of

Master of Science

Department of Mechanical Engineering

2013

This thesis entitled:
Bone Morphology and Mechanical Characteristics in Murine Models of Chronic Kidney Disease
Written by Andrew C Cureton
has been approved for the Department of Mechanical Engineering

_____
Virginia Ferguson

_____
Wei Tan

Date: _____

The final copy of this thesis has been examined by the signatories, and we find that both the content and the form meet acceptable presentation standards of scholarly work in the above mentioned discipline.

Cureton, Andrew C (M.S., Mechanical Engineering)

Bone Morphology and Mechanical Characteristics in Murine Models of Chronic Kidney Disease

Thesis directed by Professor Virginia L. Ferguson

The aim of this thesis is to investigate the changes in the bone tissue of mice that occur as a result of Chronic Kidney Disease (CKD). Due to the disruptions in mineral homeostasis and metabolism that result from loss of renal function, individuals with CKD are at a higher risk of bone fracture. In order to study the relationship between CKD and bone responses two surgical models of CKD are used herein: uninephrectomy (UNx) and 5/6 nephrectomy (5/6Nx). In general, surgically induced CKD was accompanied with a decrease in bone quality as measured by μCT morphological analysis, mechanical testing, and quantitative histomorphometry. In male C57BL/6 mice aged 4 months, trabecular number (Tb.N) decreased and trabecular spacing (Tb.Sp) increased 8 weeks after UNx ($p > 0.10$), however no statistically significant changes in bone strength or microarchitecture were observed after UNx. Eight weeks after 5/6Nx, a model of moderate to severe CKD, male C57BL/6 and FVB mice showed significant decrease in bone mineral density and cortical thickness, although no changes in mechanical properties were observed. Overall, these changes were shown to be compartment and site-specific and reveal that the effects of CKD on bone tissue are complex and variable. Further investigation of the time course of the diseased state as well as dietary phosphate loads must be considered when researching bone effects of CKD in murine models.

Contents

1. Background

1.1 Chronic Kidney Disease and Mineral Homeostasis

Chronic Kidney Disease (CKD) can describe a variety of conditions in which the structure and function of the kidneys are affected. The exact pathogenesis of CKD can vary from individual to individual, but the definition of CKD is based on decreased kidney function as measured by glomerular filtration rate (GFR). (Table 1) [1] Surprisingly, only 26% of the US population over the age of 70 has normal kidney function (>90 mL/min), while 49% has mildly decreased (60-89 mL/min) and 25% has moderately decreased kidney function (30-59 mL/min). [2]

Table 1: Definitions of Stages of CKD based on Glomerular Filtration Rates. Stage 5 is also known as End Stage Renal Disease (ESRD)

	GFR (mL/min)*
Normal	**125**
Stage 1	**>90**
Stage 2	**60-89**
Stage 3	**30-59**
Stage 4	**15-29**
Stage 5	**<15**

* Normalized to an average surface area of 1.73 m^2

One of the critical effects of the decrease in kidney function defined by CKD is a disruption of normal mineral homeostasis within the body, particularly in regards to calcium and phosphate homeostasis. These disruptions and alterations in the control pathways for calcium and phosphate homeostasis progress as kidney function decreases and can lead to secondary hyperparathyroidism (SHPT), disorders of vitamin D and calcium metabolism, hyperphosphatemia, and calcification of the vasculature. [3]

Of specific interest for this current work is the change in phosphate metabolism due to loss of renal function. The kidneys play a primary role in the complex regulatory system that governs normal phosphate homeostasis. (Figure 1) As kidney function

declines, phosphate filtration decreases, intestinal calcium absorption decreases (leading to hypocalcemia), and calcitriol levels decline–all of which lead to an increase in parathyroid hormone (PTH) and fibroblast growth factor-23 (FGF23) production. [4] The increase in serum PTH helps facilitate urinary clearance of phosphate, which restores normal phosphate homeostasis, however this restoration occurs at the expense of developing SHPT. [5] Once GFR falls below ~40 mL/min this regulatory mechanism can no longer compensate for phosphate retention due to decreased kidney function and serum phosphate levels begin to rise eventually leading to hyperphosphatemia, though not until GFR drops to the point of requiring dialysis. [3]

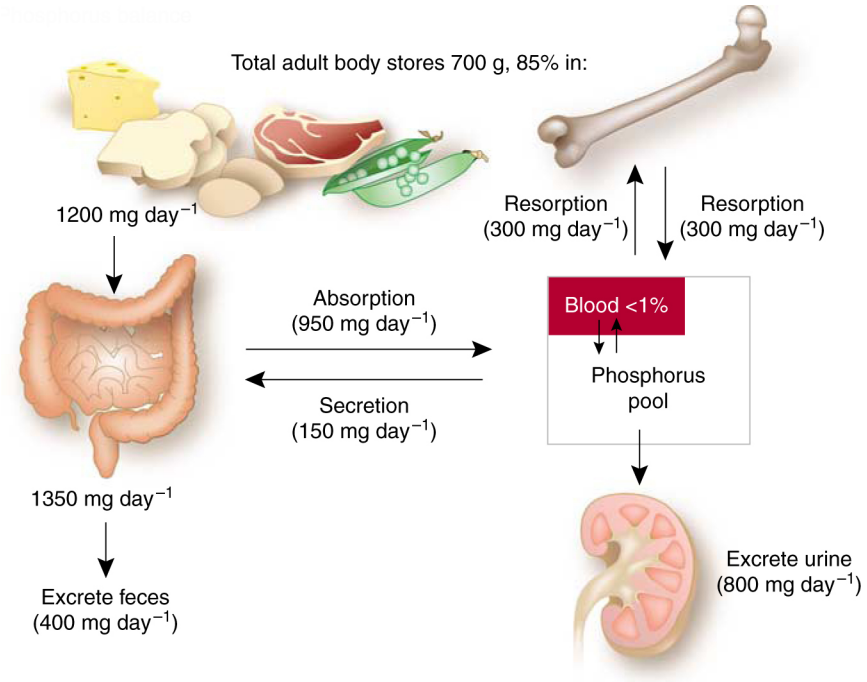

Figure 1: Phosphorus balance in normal human physiology is controlled by the kidneys, intestine, and phosphorous exchange from bone tissue. Adapted from Hruska *et al.* [6]

1.2 Murine Models in Bone Research

Mice are economical, as compared to other research animal models, easier to handle, genetically well-characterized, and even genetically manipulatable. And so mice are often the research animal models of choice when it comes to bone research. [7] The C57BL/6 (C57) strain is the most widely used inbred strain for research purposes having been well characterized including being the first to have their entire genome sequenced. As such the C57 strain has been widely used in bone research. Several studies have been undertaken to map the genetic influence on the variation in bone within the C57 strain as well as multiple other inbred strains of mice. Beamer *et al.* [8] looked at the genetic variability of bone mineral density (BMD) in 12-month old female mice from 11 inbred strains. Of the strains investigated, they were able to conclude that the C3H/HeJ (C3H) mice possessed the highest peak bone density, while the C57 mice had the lowest femoral BMD, with a value that is 50% lower than that observed in the C3H mice. In another study, 3 strains of mice were analyzed for genetic variations in bone strength, shape, and histomorphometry. [9] The C57 and C3H mice were also included in this study and it was shown that C57 mice have the thinnest cortices at the mid-diaphysis of both the femur and tibia of all the mice studied. Likewise, the C57 mice also showed impaired mechanical properties when compared to the other mice in the study, as measured in ultimate load, yield load, stiffness, ultimate stress, and yield stress. [9]

The effects of aging on the bone characteristics of inbred mice have also been well established. One study looked at the effects of aging on the bone characteristics of the C57 strain of mice exclusively, indicating that with increasing age comes an overall decrease in cortical area and thinner cortices at the femur mid-diaphysis. [10]

Furthermore, another study found trabecular microarchitecture changes with age in C57 mice by increased trabecular spacing (Tb.Sp) and decreased cancellous bone volume and trabecular number (Tb.N). [11]

While the genetic differences between inbred strains of mice enable the study of the link between specific genes and bone traits, we anticipate that similar genetic influences exist that regulate the prevalence and/or severity of kidney disease. Specifically, we believe that these genetic differences play an important role in the corresponding bone changes and other physiological alterations that result from CKD.

2. Motivation

2.1 CKD-Mineral and Bone Disorder

The disruptions in mineral homeostasis that occur as a result of decreased renal function can be manifested into a range of conditions that affect bone and mineral metabolism. These CKD associated metabolic bone disorders (CKD-MBD) can involve disequilibrium in calcium, phosphate, and PTH, or disruptions in vitamin D metabolism. As well as include abnormalities in bone turnover, mineralization, volume, linear growth, and strength. And lastly can lead to vascular calcification. [12, 13] The influence of this diseased state on bone can take two forms. First, a low-turnover metabolic bone disorder known as adynamic bone may occur. Secondly, elevated levels of PTH can lead to SHPT, which results in a high-turnover bone disease. [12] SHPT causes high bone turnover by inducing a net bone resorption, in which calcium and phosphate are liberated from bone into the blood stream in response to the disruptions in mineral homeostasis. In this case, PTH stimulates osteoclastic activity to achieve the mobilization of calcium and restore serum calcium levels. [14]

From a clinical perspective, ample evidence exists to suggest that CKD patients are at an increased risk of bone fracture. One study demonstrated that hip fracture is more strongly related to mild/moderate CKD than all other typical risk factors for bone fracture such as age, gender, body weight, and race. [15] Another study found that in male patients with stage 4 CKD the risk for hip fracture was almost 4 times higher than the risk for hip fracture among the general population without CKD, even among the older population. [16] Furthermore, Mittalhenkle *et al*. [17] reported that 1-year mortality

among dialysis patients after a hip fracture was approximately 50%, while the 1-year mortality rate for the general population after a hip fracture is less than 20%.

2.2 CKD and Bone Effects in Mice

Of the research that has been conducted regarding the bone effects of CKD in murine models, one of the most active areas of research is the investigation of vascular calcification. There have also been several studies that have looked at adynamic bone disorder (ABD) in mice. In fact, Lund *et al*. [18] successfully reversed ABD in mice with CKD, while also preventing the development of SHPT, with a bone anabolic, bone morphogenetic protein-7 (BMP-7). In regards to the proposed high-turnover bone disorder associated with CKD, which is the focus of this current work, several studies have investigated these bone changes with various models of CKD in mice. One such study looked into the effects of partial renal ablation to model CKD and the effects such a surgery had on mandibular bone in DBA/2 mice. [14] Bone microarchitecture analysis by micro-computed tomography (μCT) revealed a significant decrease in cortical thickness (Ct.Th), and an increase in trabecular thickness (Tb.Th) and trabecular bone volume-to-total volume (BV/TV) in uremic mice as compared to sham mice, regardless of a the amount of phosphate in their diet. Furthermore, they found a significant reduction in Ct.Th among sham mice between high and low phosphate diets, indicating the influence of a strong dietary phosphate load on bone metabolism. The partial renal ablation model used in Lee's *et al.* [14] study was essentially a uninephrectomy (UNx) and may be considered as an effective model for mild CKD in mice.

Another surgical model of CKD used in mice is the 5/6 nephrectomy (5/6Nx). This surgical method removes 5/6ths of the renal tissue mass and effectively establishes

severe kidney dysfunction. Kadokawa *et al*. [19] used this model in male Crlj:CD1 mice in order to study the time course of trabecular microarchitecture changes due to 5/6Nx as well as material changes in the cortical bone of the tibia. Trabecular microarchitecture measures declined with age in their study, with compounded effects seen as a result of 5/6Nx. 5/6Nx resulted in a severe decline in BV/TV and Tb.N, as well as an increase in Tb.Sp. Despite the changes observed in the trabecular analysis, Kadokawa did not observe any material changes in cortical bone parameters, as measured by nanoindentation, as a result of 5/6Nx.

3. Overarching Hypotheses and Study Design

This thesis first and foremost explores two different surgical models of CKD, UNx as a form of mild CKD and 5/6Nx as a form of moderate to severe CKD, and the resulting effects on the bone tissue from both morphological and mechanical perspectives. What follows in this thesis are two separate studies designed with both of these surgical models of CKD. The first study employs UNx as the surgical model of mild CKD in male C57BL/6 mice of two different ages (at and post skeletal maturity), and also investigates the ability of the dietary phosphate binding compound sevelamer to affect phosphate balance and mitigate deleterious bone changes. The second study utilizes 5/6Nx to model moderate to severe CKD in two different strains of mice, C57BL/6 and FVB.

The overarching hypothesis of this work is that reduced kidney volume/function in mice will negatively affect bone quality and mechanical properties, where bone quality can be defined as describing all bone parameters beyond mineral density. To test this broad hypothesis, we have designed the first study in this thesis to investigate mild CKD, hypothesizing that UNx will result in an overall decline in bone quality and mechanical properties, compounded by age effects. Because these mice were fed a typical rodent diet, we were also interested in how further reduction of the dietary phosphate load by sevelamer would affect the bone quality in these mice. We anticipated that sevelamer would reduce serum phosphate, which should reverse the effects of hyperphosphatemia and SHPT, to produce a bone phenotype more comparable to the sham group in the study.

The second study in this thesis was designed to investigate moderate to severe CKD in two different inbred strains of mice, in which we hypothesized that bone effects due to a more severe model of CKD will be more pronounced than in the UNx study. Additionally, we expected to see different responses in the bone tissue of the two strains of mice due to potential genetic influences that differ between strains, but because FVB mice have not had their bone phenotype characterized, we first wanted to provide a basis for evaluating the FVB response to 5/6Nx by characterizing the FVB bone in a non-diseased state.

4. Characterizing Bone Experimentally

4.1 Micro-computed tomography

Micro-computed tomography (μCT) is a noninvasive imaging technique that is used to characterize bone morphology of both trabecular and cortical tissues. Analysis of bone by μCT provides excellent reproducibility and allows for a high degree of accuracy in quantifying bone morphology. Benefits to using μCT for this type of analysis include: (1) the ability to make direct 3D measurements of trabecular morphology as opposed to calculating these parameters from 2D stereologic models (Table 2); (2) a larger region of interest may be analyzed within the sample as compared to 2D histological methods; (3) samples can be analyzed much faster than older methods; and (4) it is non-destructive and will leave the samples available for other assays with which to describe the bone. [20, 21]

Table 2*: Definition and Description of 3D Outcomes for Bone Morphology by μCT

Abbreviation	Variable	Description	Standard Unit
Trabecular			
TV	Total volume	Volume of the entire region of interest	mm^3
BV	Bone volume	Volume fo the region segmented as bone	mm^3
BV/TV	Bone volume fraction	Ratio of the segmented bone volume to the total volume of the region of interest	%
Conn.D	Connectivity density	A measure of the degree of connectivity of trabeculae normalized by TV	$1/mm^3$
SMI	Structural model index	An indicator of the structure of trabeculae; SMI will be 0 for parallel plates and 3 for cylindrical rods	
Tb.N	Trabecular number	Measure of the average number of trabeculae per unit length	1/mm
Tb.Th	Trabecular thickness	Mean thickness of trabeculae, asses using direct 3D methods	mm
Tb.Sp	Trabecular spacing	Mean distance between trabeculae, assessed using direct 3D methods	mm
vBMD	Volumetric bone mineral density	A description of mineral density based on the entire tissue volume	mg HA/cm^3
Cortical			
BA/TA	Bone area fraction	Ratio of the cortical bone area to the total volume of the region of interest	%
Ct.Th	Cortical thickness	Average cortical thickness	mm
pMOI	Polar moment of inertia		mm^4
TMD	Tissue mineral density	A description of mineral density based on the bone volume	mg HA/cm^3

* Adapted from Bouxsein et. al. [20]

4.2 Mechanical Testing of Bone

Because bone has been studied from a mechanical perspective for a long time, there are a variety of testing methods that are used to characterize the mechanical properties of bone. The methods chosen to characterize the mechanical properties of bone for the studies presented in this thesis are 3-point bending [22, 23] and a femoral neck fracture test [24, 25]. These two tests were chosen because they are both simple to perform, the data analysis is straightforward, and they have excellent repeatability when used to test mouse bones. Both tests also give results that are useful and meaningful from a bone mechanics characterization standpoint, as well as having less error than some of the more complex testing methods, such as torsional tests. [26] For both tests, force-deflection curves were analyzed for mechanical properties such as stiffness, load at yield, maximum load, and fracture load. (Figure 2)

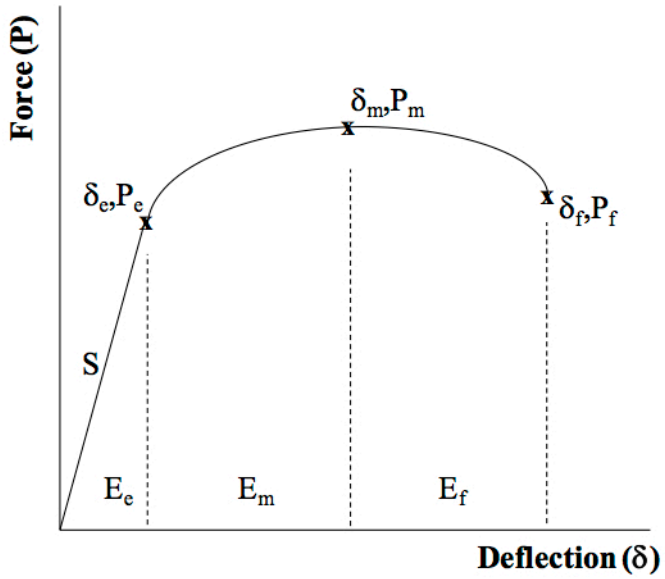

Figure 2 – Force vs. deflection curve [27]

Post yield displacement (PYD) is one additional measure that will be calculated to determine if the bone tissue becomes more or less brittle as a result of UNx. PYD is defined as the deflection that occurs after elastic yield and before fracture. Brittle bone will have lower PYD, while ductile bone will have higher PYD.

4.3 Bone Histomorphometry

The mice in both of the studies herein were administered calcein and tetracycline labels at a designated date prior to sacrifice. Calcein and tetracycline are both fluorochrome dyes, that when administered to mice, will bind to calcium prior to bone apposition. [28] In order to make histomorphometric measures, embedded and sectioned bone samples are examined under a fluorescent microscope. Any bone apposition that has occurred since the labels were administered will fluoresce under the scope and allow for quantitative measurement of many histomorphometric measures, both dynamic and non-dynamic. (Figure 3)

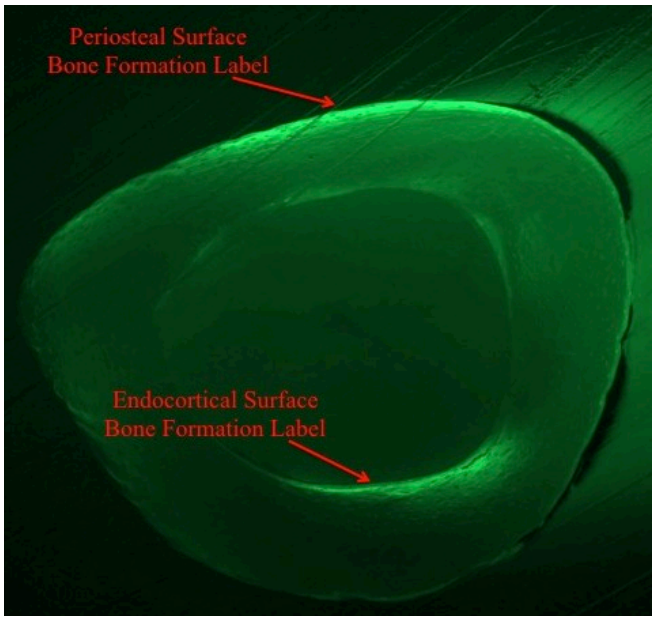

Figure 3 – Sample quantitative histomorphometry image showing labeled bone apposition on both the periosteal and endocortical surfaces.

Dynamic measures include active mineralizing perimeter (AMP), bone formation area (BFA), bone formation rate (BFR), and mineral apposition rate (MAR), all of which can be applied to both periosteal and endocortical surfaces. Non-dynamic measures include average cortical thickness (Ct.Th), periosteal and endocortical perimeters (Ps.P and Ec.P), bone area (BA), and endocortical area (Ec.A).

4.4 Compositional Analysis

Ashing was performed on the bones of the 5/6Nx study to enable calculation of mineral content in the bones. This assay gives us another means of quantifying the degree of mineralization in the bone, and is important because we know that decreases in mineral content in bone will be accompanied by a decrease in mechanical properties. [29] In order to make this calculation, the bones are dried at two different temperatures and massed in order to determine both the dry mass and the mineral mass of the bone. The mineral percent composition of the bone can then be calculated from these to values by using the relationship:

$$\%Min = \frac{Min_M}{Dry_M} \times 100\%$$

4.5 Gene Expression Analysis

Because of the complex nature of CKD and mineral homeostasis, another useful method of characterizing the diseased state in mice is to explore the gene expression changes that result from loss of renal function. There are many key molecular players involved in the pathways that govern mineral homeostasis and as such, they were not exhaustively studied in this thesis. Several genes of interest were studied, however, with the hope of further understanding the nature of CKD's effect on bone.

Bone is a dynamic material that can respond to a variety of impulses to direct remodeling. This bone remodeling can involve either bone resportion by osteoclasts or bone synthesis by osteoblasts, the two primary cellular components of bone remodeling. [30] Several proteins control osteoclast differentiation, or osteoclastogenesis. Receptor activator of NF-κB ligand (RANKL) and osteoprotegerin (OPG) are competitive antagonists involved in osteoclast activation, both binding to the receptor activator of NF-κB (RANK). Osteoclast activation occurs when RANKL binds with RANK, however, OPG is a decoy receptor for RANKL and therefore a negative regulator of osteoclastogenesis. Therefore, the ratio between RANKL and OPG expression determines the level of osteoclast activation and function within the bone tissue. [30, 31] It is this relationship that was explored in this thesis and although there are many more genes/proteins involved in the bone remodeling and mineral metabolism pathways, these genes were selected to provide at least a brief picture of the gene expression changes that occur as a result of loss of renal function.

5. Study 1: The Effect of Age and Sevelamer on the Bone of Uninephrectomized Mice

5.1 Introduction

The objective of this study is to distinguish the effects of uninephrectomy (UNx) and sevelamer, a dietary phosphate binder, on the bone of both mature and old C57 mice. In order to gain a full picture of the quality of the bone within these mice, their bones were analyzed from both morphological and mechanical perspectives.

The bone characteristics of C57 mice have been well documented with the bone effects of aging having been studied in the past. [10, 11] Several studies have also looked at the bone effects of CKD in the C57 strain. Among those studies Lund *et al*. [18] performed UNx on C57 mice and concluded that restricting dietary phosphate and administering calcitriol both play a role in maintaining normal mineral homeostasis and preventing secondary hyperparathyroidism (SHPT) associated with CKD. In this setting, an adynamic bone disorder characterized by low bone turnover develops due to the lack of SHPT. [12] Our current study was designed to test the ability of sevelamer to reduce serum phosphate in uninephrectomized C57 mice in order to better understand the role of phosphate regulation in the bone-kidney axis of mice.

We hypothesized that UNx will induce a mild case of CKD in the C57 mice as measured by blood serum biochemical levels. Furthermore, we expected this mild CKD to disrupt normal mineral homeostasis in the mice resulting in a decrease in bone quality as measured in both morphological assays and mechanical testing. The addition of sevelamer should help maintain phosphate homeostasis, and as such could have the effect of controlling serum PTH levels and reversing the bone effects of decreased renal

function. Age was expected to exasperate the effects seen in the younger group, with bone quality declining even more drastically with increased age.

5.2 Materials and Methods

A total of n = 47 male mice aged 4 months (skeletally 'mature') and 22 months (skeletally 'old') were obtained from the NIA and housed in our animal facility. Within each age group mice were either subjected to a sham surgery, UNx, or UNx plus sevelamer therapy. (Table 3)

Table 3: Study Design

Mature Control *n = 9*	Mature UNx *n = 8*	Mature UNx + Sev *n = 8*
Old Control *n = 9*	Old UNx *n = 6*	Old UNx + Sev *n = 8*

5.2.1 Animal Preperation

4-month and 22-month old male C57BL/6J mice were obtained from National Institute of Aging (Bethesda, MA). They were maintained on a 12-h light/12-h dark cycle. After one month mice underwent left unilateral nephrectomy (UNx). In the control mice, a sham operation was performed. Mice were maintained on chow diet only or 2% sevelamar carbonate (Genzyme, Framingham, MA) mixed in chow diet for 8 weeks.

Animal studies and relative protocols were approved by the Animal Care and Use Committee at the University of Colorado Denver.

5.2.2 Serum Biochemistry

Plasma creatinine concentrations were determined using kits from BioAssay System (Hayward, CA). Blood urea nitrogen (BUN), plasma phosphate and plasma calcium levels were measured with kits from Stanbio Laboratory (Boerne, TX). Intact plasma PTH level was measured with kits from Immutopics (San Clemente, CA). The FGF23 kit from Kainos Laboratories (Tokyo, Japan) was used to determine plasma FGF23 level.

5.2.3 Micro-computed Tomography

The left tibiae were cleaned and stored in 70% ethanol at 4 ^{o}C for subsequent analysis of trabecular microarchitecture using micro-computed tomography (μCT; 9 μm voxel size; MicroCT 80, Scanco Medical AG; Basserdorf, Switzerland). Tibia trabecular bone parameters were obtained from scans extending in the distal direction from immediately below the proximal growth plate. The proximal tibia was evaluated for parameters including trabecular bone volume fraction (BV/TV), trabecular number (Tb.N), trabecular spacing (Tb.Sp), trabecular thickness (Tb.Th), volumetric bone mineral density (vBMD), structural model index (SMI), and connectivity density (Conn.D). The left femurs were cleaned and fresh frozen in phosphate buffered saline (PBS) soaked gauze. These femurs were thawed and scanned (9 μm voxel size) at the mid-diaphysis and μCT bone parameters quantified included BV/TV, bone area-to-total area (BA/TA), cortical thickness (Ct.Th), tissue mineral density (TMD), and polar moment of inertia (pMOI).

5.2.4 Mechanical Testing

Following μCT analysis the left femurs were refrozen in PBS soaked gauze at -20 ^{o}C. Prior to testing the femurs in a three-point bending system (MTS Insight II, 2 kN load cell; Mechanical Testing Systems, Eden Prairie, MN), the bones were allowed to defrost at 4 ^{o}C overnight. The samples were tested to failure using a deflection rate of 5 mm/min on a custom anvil with an 8-mm span. Force-deflection curves were analyzed for mechanical properties that include stiffness, load at yield, maximum load, and fracture load as in Ferguson *et al.* [10]

After the three-point bending tests the proximal femur fragment was secured in a pen-vise that was vertically mounted on a base plate and oriented such that a flat compression plate would contact only the femoral head. The femoral neck was tested to failure (MTS Insight II; 2 kN load cell) at a deflection rate of 5 mm/min similar to Jämsä *et al.*[24] Visual observation confirmed that the femoral neck was subjected to compressive force acting directly onto the femoral head inline with the anatomical axis of the femur. Force-deflection curves were analyzed for mechanical properties that include load at yield, maximum load, and fracture load.

5.2.5 Bone Histomorphometry

Following μCT analysis the left tibiae were histologically dehydrated in ethanol (to a maximum of 100%), cleared in acetone, and then embedded in poly(methyl methacrylate) (PMMA; Sigma-Aldridge). The PMMA-embedded tibiae were sectioned at 0.8 mm proximal to the tibia-fibula junction using a low-speed diamond blade saw (Buehler; Lake Bluff, IL). The exposed surface on the proximal face of the sectioned tibia was then polished to a 3 μm finish using aluminum oxide pastes on rayon fine clothes

(South Bay Technologies; San Clemente, CA). Each sectioned bone cross-section was imaged on a UV microscope (Zeiss Axioskop 40FL; Jena, Germany) with a DAPI/FITC/TRITC filter (69000 – ET; Chroma Technology Corp; Bellows Falls, VT). The images were analyzed for bone area, periosteal perimeter, and endocortical area.

5.2.6 Statistical Analysis

All data were analyzed using a one-way ANOVA and post-hot Tukey's HSD tests using JMP Pro version 10.0.1 software (SAS Institute, Inc.; Cary, NC). T-tests comparing sham groups between the mature and old age mice were also done using JMP.

5.3 Results

5.3.1 Serum Biochemistry

Among the blood serum biochemical data, the only significant changes observed due to either UNx or UNx and Sevelamer were seen in the FGF23 data in the mature mice. As a result of UNx, circulating FGF23 in the mature mice increased 94.7% as compared to the sham group, while in the UNx group that received sevelamer circulating FGF23 increased 81.3% as compared to the sham group. (Table 4)

Table 4: Blood serum biochemical data. All data is presented as mean ± SD.

	Mature		
	Sham	**UNx**	**UNx+Sev**
Plasma Pi	**6.49 ± 0.91**	**6.21 ± 1.24**	**5.94 ± 1.13**
Serum FGF23	**249.20 ± 41.92**	**485.27 ± 102.96 §**	**451.78 ± 91.55 §**
Plasma PTH	**568.71 ± 263.43**	**622.55 ± 198.13**	**717.33 ± 336.58**
	Old		
	Sham	**UNx**	**UNx+Sev**
Plasma Pi	**6.0508 ± 1.4173**	**6.06 ± 2.07**	**6.97 ± 3.07**
Serum FGF23	**330.7890 ± 100.3868**	**510.09 ± 108.99**	**588.40 ± 411.89**
Plasma PTH	**379.1357 ± 137.2048**	**668.11 ± 298.76**	**452.79 ± 193.13**

§ $p < 0.001$ for comparison with sham group

5.3.2 Bone microarchitecture

Bone microarchitecture outcomes among both trabecular and cortical analysis illustrated the effect of age on bone quality in these mice. (Table 5) The old sham mice showed a 46.3% decrease in BV/TV, a 40.4% decrease in Tb.N, a 77.4% increase in Tb.Sp, a 3.2% decrease in Tb.Th (N.S.), and a 51.3% decrease in vBMD as compared to the mature sham mice. Among the cortical outcomes the old sham mice showed a 10.0% decrease in Ct.Th, a 7.6% increase in pMOI (N.S.), and a 2.7% increase in TMD as compared to the mature sham mice.

Among the mature mice Tb.N and Tb.Sp appear to be trending towards the expected outcome as a result of UNx ($0.05 < p < 0.1$), with Tb.N decreasing 9.6% and Tb.Sp conversely increasing 12.7% in the sham groups as compared to the UNx groups. No significant changes in bone microarchitecture were observed in the old mice as a result of UNx. Likewise, sevelamer appears to have not had any significant effect on the bone microarchitecture outcomes of either trabecular or cortical bone.

5.3.3 Mechanical Properties

The decrease in bone quality as a result of age has been confirmed among 3-pt bending test outcomes with the old sham mice showing a 31.2% decrease in yield strength, a 29.9% decrease in max load, a 25.6% decrease in fracture load, and a 42.6% decrease in stiffness as compared to the mature sham. (Table 6) Among femoral neck test outcomes, only load at yield and max load showed significant changes between sham groups with a 38.8% decrease and 34.3% decrease in the old sham group as compared to the mature sham mice, respectively.

Table 5: Micro-computed tomography data for both trabecular and cortical bone presented as mean ± standard deviation. The trabecular data is from analysis of the proximal tibia and the cortical data is from analysis of the femur mid-diaphysis.

	Mature			Old		
	Sham (n = 9)	UNx (n = 8)	UNx+Sev (n = 8)	Sham (n = 8)	UNx (n = 6)	UNx+Sev (n = 8)
Trabecular						
BV/TV (%)	9.04 ± 2.00	8.60 ± 1.49	8.64 ± 1.59	4.85 ± 2.49 §	3.72 ± 1.30	2.93 ± 0.72
Tb.N	3.94 ± 0.30	3.56 ± 0.44 †	3.80 ± 0.30	2.35 ± 0.46 §	2.22 ± 0.35	2.29 ± 0.33
Tb.Sp (mm)	0.25 ± 0.02	0.28 ± 0.03 †	0.26 ± 0.02	0.45 ± 0.11 §	0.46 ± 0.08	0.45 ± 0.06
Tb.Th (mm)	0.0439 ± 0.0031	0.0427 ± 0.0017	0.0439 ± 0.0029	0.0425 ± 0.0078	0.0444 ± 0.0059	0.0441 ± 0.0081
vBMD (mg HA/cc)	151.52 ± 29.34	147.98 ± 21.69	152.59 ± 23.92	73.78 ± 39.60 §	60.33 ± 21.42	48.44 ± 12.68
Cortical						
Ct.Th (mm)	0.20 ± 0.02	0.19 ± 0.01	0.19 ± 0.004	0.18 ± 0.02 §	0.15 ± 0.02	0.16 ± 0.02
pMOI (mm^4)	0.51 ± 0.05	0.56 ± 0.10	0.50 ± 0.05	0.55 ± 0.06	0.55 ± 0.12	0.54 ± 0.06
TMD (mg HA/cc)	1,072.98 ± 31.88	1,086.86 ± 21.90	1,070.95 ± 31.72	1,102.39 ± 29.58 *	1,081.77 ± 32.70	1,094.57 ± 30.96

† $p < 0.10$ for Tukey's HSD between sham and UNx group. § $p < 0.002$ for t-test between mature sham and old sham mice.
* $p = 0.0685$ for t-test between mature sham and old sham mice.

Table 6: 3-pt bending of the femur and femoral neck test data presented as mean ± standard deviation.

	Mature			Old		
	Sham	UNx	UNx+Sev (n = 8)	Sham (n = 6)	UNx	UNx+Sev
3-pt Bending Test						
Load at Yield (N)	17.31 ± 2.06 (n = 9)	19.34 ± 1.68 (n = 7)	17.75 ± 3.11	11.91 ± 2.86 §	13.48 ± 3.10 (n = 6)	10.87 ± 1.32 (n = 8)
Max Load (N)	19.30 ± 2.27 (n = 9)	20.92 ± 1.53 (n = 7)	18.87 ± 2.85	13.53 ± 2.38 §	14.15 ± 2.98 (n = 6)	13.24 ± 2.57 (n = 8)
Fracture Load (N)	11.97 ± 2.90 (n = 9)	13.74 ± 3.68 (n = 7)	15.75 ± 3.92	8.90 ± 2.60 †	10.70 ± 3.77 (n = 6)	9.57 ± 4.36 (n = 8)
Stiffness (N/mm)	123.05 ± 16.19 (n = 9)	131.21 ± 21.28 (n = 7)	126.79 ± 17.92	70.64 ± 21.60 §	64.76 ± 24.10 (n = 6)	10.87 ± 1.32 (n = 8)
Femoral Neck Test						
Load at Yield (N)	17.62 ± 4.60 (n = 8)	13.57 ± 6.42 (n = 8)	14.82 ± 3.74	10.79 ± 3.88 §	9.87 ± 3.77 (n = 5)	11.42 ± 2.96 (n = 6)
Max Load (N)	23.94 ± 2.21 (n = 8)	24.88 ± 2.57 (n = 8)	23.15 ± 1.95	15.72 ± 3.42 §	15.43 ± 2.94 (n = 5)	14.42 ± 1.47 (n = 6)
Fracture Load (N)	19.09 ± 7.63 (n = 8)	21.32 ± 6.40 (n = 8)	21.67 ± 4.58	14.49 ± 3.39	14.80 ± 3.47 (n = 5)	14.16 ± 1.53 (n = 6)
Stiffness (N/mm)	140.47 ± 66.24 (n = 8)	144.13 ± 37.19 (n = 8)	152.88 ± 44.36	104.56 ± 37.73	120.36 ± 26.02 (n = 5)	125.79 ± 33.25 (n = 6)

§ $p < 0.05$ for t-test between mature and old sham mice. † $p < 0.1$ for Tukey's HSD between sham and UNx group within that age.

5.3.4 Quantitative Histomorphometry

Non-dynamic measures of cortical bone area, endocortical area, and periosteal perimeter were collected on all samples. Analysis was limited to the mature and the old sham groups only. (Table 7) This data also confirms the effects of aging on the bones of these C57 mice with cortical bone area decreasing 15.8%, endocortical area increasing 41.3%, and periosteal perimeter increasing 2.0% in the old sham mice when compared to the mature sham mice.

Some samples did show labeled bone apposition on either the periosteal and/or the endocortical surfaces, however most did not. To add to the complications, the PMMA embedding process proceeded in a peculiar manner in this study. Large quantities of samples were ruined in the embedding process and were discarded from any further analysis. The original assay for this portion of the experiment was therefore adapted once analysis of these images began due to the highly variable results. It was not possible to get meaningful data on bone and mineral apposition rates because within each group there was simply too much variability between samples.

Table 7: Non-dynamic quantitative histomorphometry data presented as mean ± standard deviation.

	Mature Sham	Old Sham
Bone Area (mm2)	**0.73 ± 0.04**	**0.62 ± 0.07 §**
Endocortical Area (mm2)	**0.48 ± 0.05**	**0.68 ± 0.20 §**
Periosteal Perimeter (mm)	**4.07 ± 0.16**	**4.15 ± 0.34**

§ $p < 0.05$ for t-test between mature sham and old sham mice.

5.4 Preliminary Assessment of Results

The objective of this study was to determine the morphological and mechanical changes in mature and old C57 mice as a result of UNx and UNx plus the dietary

phosphate binder sevelamer. It was expected that morphological and mechanical properties would decline as a result of UNx, while sevelamer would mute some of those effects by improving blood serum phosphate levels. It was also expected that age would have a compounding effect on the changes due to UNx in the mice, with the old mice showing both a decline in morphological measures as well as a decrease in mechanical strength measures.

The already well-documented effects of aging on the bone quality of C57 mice were confirmed in both morphological analysis and mechanical testing. However no statistically significant changes were observed as a result of either UNx or sevelamer therapy. This is likely due to the time course of the UNx in these mice. Bone tissue responds slowly to loss of renal function in C57 mice and in order to see more pronounced changes the mice must be maintained with UNx for longer than the 8 weeks that was allowed in this current study. Additionally, loss of one entire kidney might not model severe enough of a decline in renal function to elicit bone changes. Human physiology can adapt to the loss of one kidney quite well, and as such mice might also be able to compensate effectively for the loss of one kidney. These mice were also fed a normal chow diet, where a high dietary phosphate load could further stress the mineral disequilibrium as a result of loss of renal function, resulting in more pronounced changes in the bone tissues.

6. Study 2: Bone Morphology and Mechanics After 5/6 Nephrectomy in Two Inbred Strains of Mice

6.1 Introduction

Currently there is much interest in the effects of renal failure on bone quality and strength, certainly from a research perspective, but even more so from a clinical one. In the US, incidence of Chronic Kidney Disease (CKD) is nearly 400 million cases per million citizens and with an average survival of 3-5 years, prevalence is nearing 1800 cases per million. Additionally, millions more are at an increased risk of developing the disease due to old age, diabetes, hypertension, obesity, and cardiovascular disease. [1] CKD is a systemic affliction that has far reaching effects within the vascular, cardiac, and skeletal systems. Under normal physiological conditions there is a complex interplay between these systems in regards to mineral homeostasis and metabolism. CKD disrupts these normal processes and as a result patients with CKD are at a higher risk of bone fracture. [3, 32, 33]

Loss of renal function leads to a dysregulation of normal mineral homeostasis. Specifically, the disequilibrium of calcium and phosphate blood serum levels results in elevated parathyroid hormone (PTH) within the bloodstream and therefore secondary hyperparathyroidism (SHPT). [3] SHPT leads to an increase in bone resorption and turnover, liberating calcium and phosphate from the bone into the bloodstream. This constitutes one current explanation for the increase in bone fragility among patients with CKD. [12] Bone research plays a critical role in discerning the details of the effects of CKD on bone and like many bone research fields murine models are the research subjects of choice. [7]

Among murine models used for bone research several strains have been exhaustively characterized and their bone quality is well documented. With the goal of finding mice strains with a genetic makeup that will mimic the effects of CKD in humans, new inbred strains of mice must be explored as candidates for CKD-bone research. The genetic influence on bone quality and strength has been well documented for many strains of inbred mice. [8, 9, 34] In the case of this current research, a commonly used inbred strain was selected (C57BL/6) as well as a strain known for being useful in producing transgenic mice (FVB). The C57BL/6 (C57) strain is the most widely used inbred strain for research purposes. As such C57 mice have been well-characterized including being the first to have their entire genome sequenced. It is well documented that C57 mice possess low bone density and mineral content, thin cortices at the femur mid-diaphysis, poor mechanical properties, as well as decreasing bone quality with age. [8-10, 35] Because of the extent of their use in bone research as a strain for modeling low bone density the C57 strain was similarly selected for this study. The bone characteristics of FVB mice, however, are largely absent from the literature. This strain is known for its reproductive performance, large litter sizes, as well as having large pronuclei in the fertilized eggs, which allows for easy microinjection of DNA for creating transgenic mice efficiently. [36]

Along with the general bone characteristics of the FVB strain little is known about the bone response of both FVB and C57 mice to 5/6 nephrectomy (5/6Nx), an established model of moderate kidney disease. [19] With the removal of a significant fraction of kidney tissue from these mice it will be possible to characterize how moderate kidney disease affects bone quality while also allowing for a comparison of the bone

characteristics and response to 5/6Nx within these two inbred strains of mice. We undertook this study in order to accomplish both of these goals. Specifically, we wanted to provide a comparison between an inbred strain of mice of noted low bone quality and an inbred strain relatively unstudied from a bone perspective. Secondly, we wanted to add to the understanding of the bone-kidney axis in a state of moderate kidney disease by way of analyzing the affects of 5/6Nx on the bone of both strains of mice. We hypothesized that the FVB mice have even lower bone quality than the C57 mice and because of their genetic characteristics, reproductive performance, and ease of producing transgenic mice, could serve as an additional option for a murine model in bone research. Additionally, we hypothesize that we will see bone quality decrease in both morphological metrics and under mechanical loading in both strains as a result of 5/6Nx and the associated mineral dysregulation.

6.2 Materials and Methods

6.2.1 Animal Preparation

8-week old male C57BL/6J and FVB/J mice were obtained from The Jackson Laboratories (Bar Harbor, ME). They were maintained on a 12-h light/12-h dark cycle. At 12-weeks old, mice were 5/6 nephrectomized by the ablation of two-thirds mass of the right kidneys and subsequent left unilateral nephrectomy after one week. In the control mice, a sham operation was performed. Mice were maintained on a normal chow diet for 8 weeks. To determine the mineralization apposition rates and measure the active bone forming surfaces, calcein (10 mg/kg; Sigma) and tetracycline (20 mg/kg; Sigma) were injected intraperitoneally at 12 days and 2 days before sacrifice, respectively. Animal studies and relative protocols were approved by the Animal Care and Use Committee at

the University of Colorado Denver.

6.2.2 Serum Biochemistry

Plasma creatinine concentrations were determined using kits from BioAssay System (Hayward, CA). Blood urea nitrogen (BUN), plasma phosphate and plasma calcium levels were measured with kits from Stanbio Labporatory (Boerne, TX)

6.2.3 Micro-computed tomography

The left tibiae were cleaned and stored in 70% ethanol at 4 ^{o}C for subsequent analysis of trabecular microarchitecture using micro-computed tomography (μCT; 9 μm voxel size; MicroCT 80, ScanCo Medical AG; Basserdorf, Switzerland). Tibia trabecular bone parameters were obtained from scans extending in the distal direction from immediately below the proximal growth plate. The proximal tibia was evaluated for parameters including trabecular bone volume fraction (BV/TV), trabecular number (Tb.N), trabecular spacing (Tb.Sp), trabecular thickness (Tb.Th), volumetric bone mineral density (vBMD), structural model index (SMI), and connectivity density (Conn.D). The left femurs were cleaned and fresh frozen in phosphate buffered saline (PBS) soaked gauze. These femurs were thawed and scanned (9 μm voxel size) at the mid-diaphysis and μCT bone parameters quantified included BV/TV, bone area-to-total area (BA/TA), cortical thickness (Ct.Th), tissue mineral density (TMD), and polar moment of inertia (pMOI).

6.2.4 Mechanical Testing

Following μCT analysis the left femurs were refrozen in PBS soaked gauze at -20 ^{o}C. Prior to testing the femurs in a three-point bending system (MTS Insight II, 2 kN load cell; Mechanical Testing Systems, Eden Prairie, MN) the bones were allowed to defrost

at 4 ^{o}C overnight. The samples were tested to failure using a deflection rate of 5 mm/min on a custom anvil with an 8-mm span. Force-deflection curves were analyzed for mechanical properties that include stiffness, load at yield, maximum load, and fracture load as in Ferguson *et al.* [10]

After the three-point bending tests the proximal femur fragment was secured in a pen-vise that was vertically mounted on a base plate and oriented such that a flat compression plate would contact only the femoral head. The femoral neck was tested to failure (MTS Insight II; 2kN load cell) at a deflection rate of 5 mm/min similar to Jämsä *et al.* [24] Visual observation confirmed that the femoral neck was subjected to compressive force acting directly onto the femoral head inline with the anatomical axis of the femur. Force-deflection curves were analyzed for mechanical properties that include load at yield, maximum load, and fracture load.

6.2.5 Bone Histomorphometry

Following μCT analysis the left tibiae were histologically dehydrated in ethanol (to a maximum of 100%), cleared in acetone, and then embedded in poly(methyl methacrylate) (PMMA; Sigma-Aldridge). PMMA-embedded tibiae were sectioned at 0.8 mm proximal to the tibia-fibula junction using a low-speed diamond blade saw (Buehler; Lake Bluff, IL). The exposed surface on the proximal face of the sectioned tibia was then polished to a 3 μm finish using aluminum oxide pastes on rayon fine cloths (South Bay Technologies; San Clemente, CA). Each sectioned bone cross-section was imaged on a UV microscope (Zeiss Axioskop 40FL; Jena, Germany) with a DAPI/FITC/TRITC filter (69000 – ET; Chroma Technology Corp; Bellows Falls, VT). Each bone cross-section was analyzed for mean cortical thickness, bone formation area (BFA), bone formation

rate (BFR), and mineral apposition rate (MAR) on both the periosteal and the endocortical surfaces.

6.2.6 Gene Expression Analysis

The right femur from each animal was powdered (Sartorious mikro-dismembrator S) for gene expression by 2 subsequent 30-second intervals at 2600 rpms per the manufacture's instructions. Following powdering, RNA extraction was achieved using the QiAzol® Lysis Reagent and chloroform precipitation method (RNeasy® Lipid Tissue mini kit) and filtered using a Qiagen multichannel column per the manufacture's protocol. RNA was transcribed to cDNA using a reverse transcriptase (supertranscript II) and thermocycler (Applied biosystems Gene Amp® PCR systems 9700) starting with initiation at 25 °C for 10 minutes, followed by 37 °C for 120 minutes, and finally 85 °C for 5 minutes. Using the fast SYBR green real time RT-PCR method (Applied Biosystems, One Step), cDNA was quantified using forward and reverse primers. PCR conditions were set at an initiation temperature of 95 °C for 20 seconds, followed by 40 cycles of denaturing at 95 °C for 3 seconds and annealing at 60 °C for 30 seconds. The results were analyzed using the ΔΔCT for relative fold change using 18s as the control gene.

6.2.7 Compositional Analysis

Due to limited availability of hind limb long bones, humeri were used to do mineral compositional analysis through an ashing assay. The humeri were first oven-dried at 105 ^{o}C for 24 hours and weighed to obtain the bone dry mass. The bones were then oven-dried at 800 ^{o}C for 24 hours to obtain the bone mineral mass. Percent mineralization was calculated from these two values.

6.2.8 Statistical Analysis

All data except gene expression data were analyzed with a two-way ANOVA and post-hoc Tukey's Honestly Significant Difference (HSD) tests using JMP Pro version 10.0.1 software (SAS Institute, Inc., Cary, NC). Gene expression data (ΔC_T) were analyzed with one-way ANOVA using SigmaPlot version 11.2 software (SysStat Software, Inc., San Jose, CA).

6.3 Results

6.3.1 5/6 Nephrectomy

In order to confirm impaired kidney function serum blood urea nitrogen (BUN) and creatinine levels were taken 8 weeks after performing the 5/6Nx surgeries. (Table 8) Both C57 and FVB mice showed significant increase in both BUN (+502% and +690%, respectively) and creatinine (+35.3%, +57.5%) serum levels with 5/6Nx. However, calcium and phosphate levels remained unchanged between the sham groups and the 5/6Nx groups in both strains. And while mean PTH values illustrate a trend towards increased blood serum PTH following 5/6Nx, no statistically significant differences were observed due to high standard deviations and low number of measured samples per group.

While significant changes in trabecular microarchitecture as a result of 5/6Nx were not observed, changes in Ct.Th and TMD at the femur mid-diaphysis were detected. The FVB 5/6Nx mice had 4.0% thinner cortices at the femur mid-diaphysis and 1.9% lower TMD than the sham group. Likewise, the C57 5/6Nx mice had 10.4% thinner cortices at the femur mid-diaphysis and 1.9% lower TMD than the sham group as well. Bone mechanical properties from the 3-point bending and femoral neck tests were

unaffected in both FVB and C57 mice after 5/6Nx. The gene expression profiles for each strain in response to 5/6Nx were nearly opposite. In the C57 mice, RANKL and OPG showed a 1.39 and 1.52 fold increase in expression, respectively after 5/6Nx, while the FVB mice showed 2.13 and 3.22 fold decreases in expression of the same genes. Both strains did show a decrease in FGF23 expression with C57 expression decreasing 2.10 fold and FVB expression decreasing 4.51 fold after 5/6Nx. (Figure 4)

Table 8 – Blood serum biochemical data. All data is presented as mean ± SD.

	FVB		C57	
	Sham	*5/6 Nx*	*Sham*	*5/6 Nx*
BUN (mg/mL) **	8.93 ± 5.31 (n = 6)	70.63 ± 14.03 (n = 6) §	7.42 ± 5.68 (n = 6)	44.68 ± 8.68 (n = 6) §
Creatinine (mg/mL)	0.31 ± 0.04 (n = 8)	0.46 ± 0.04 (n = 6) †	0.37 ± 0.15 (n = 8)	0.50 ± 0.06 (n = 8) *
PTH (pg/mL)	318.41 ± 100.27 (n = 5)	528.20 ± 256.77 (n = 5)	211.12 ± 137.99 (n = 6)	301.13 ± 86.31 (n = 5)
Ca (mg/mL)	8.65 ± 0.31 (n = 8)	8.64 ± 0.25 (n = 8)	9.05 ± 1.56 (n = 8)	9.14 ± 0.46 (n = 8)
Pi (mg/mL)	8.16 ± 1.30 (n = 8)	8.93 ± 1.11 (n = 8)	8.68 ± 2.05 (n = 7)	8.52 ± 1.39 (n = 8)

§ $p < 0.0001$ for comparison between sham and 5/6Nx groups. † $p < 0.02$ for comparison between sham and 5/6Nx groups. * $p < 0.09$ for comparison between C57 sham and C57 5/6Nx. ** ANOVA Interaction $p < 0.05$.

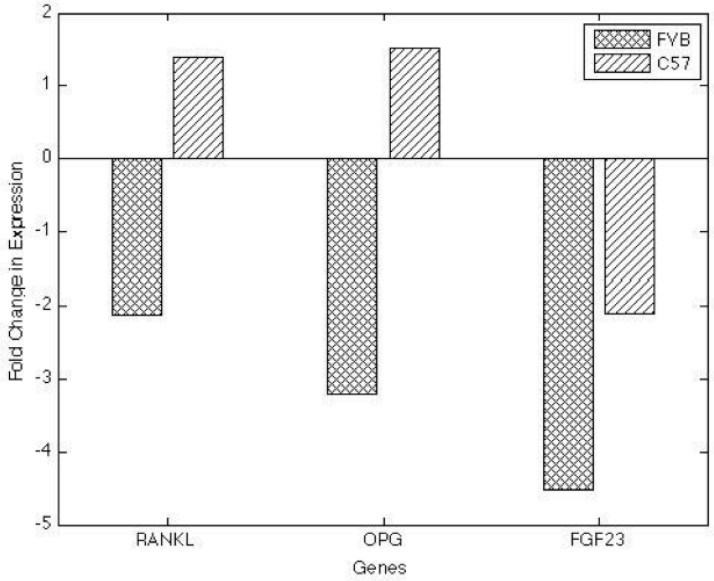

Figure 4 – Fold change in gene expression as compared to sham groups within each strain as a result of 5/6Nx.

6.3.2 Strain Comparison

While the C57 strain exhibits the expected low bone quality phenotype, the FVB strain exhibits a further decline in trabecular morphology and cortical bone quality that occurs concomitant with reduced mechanical properties. The most pronounced differences between the C57 and FVB strains were seen in the trabecular microarchitecture analysis done by μCT. Visual inspection of representative 3D images of the trabecular bone from the proximal tibia for each group of mice indicates that result from a qualitative perspective. (Figure 5)

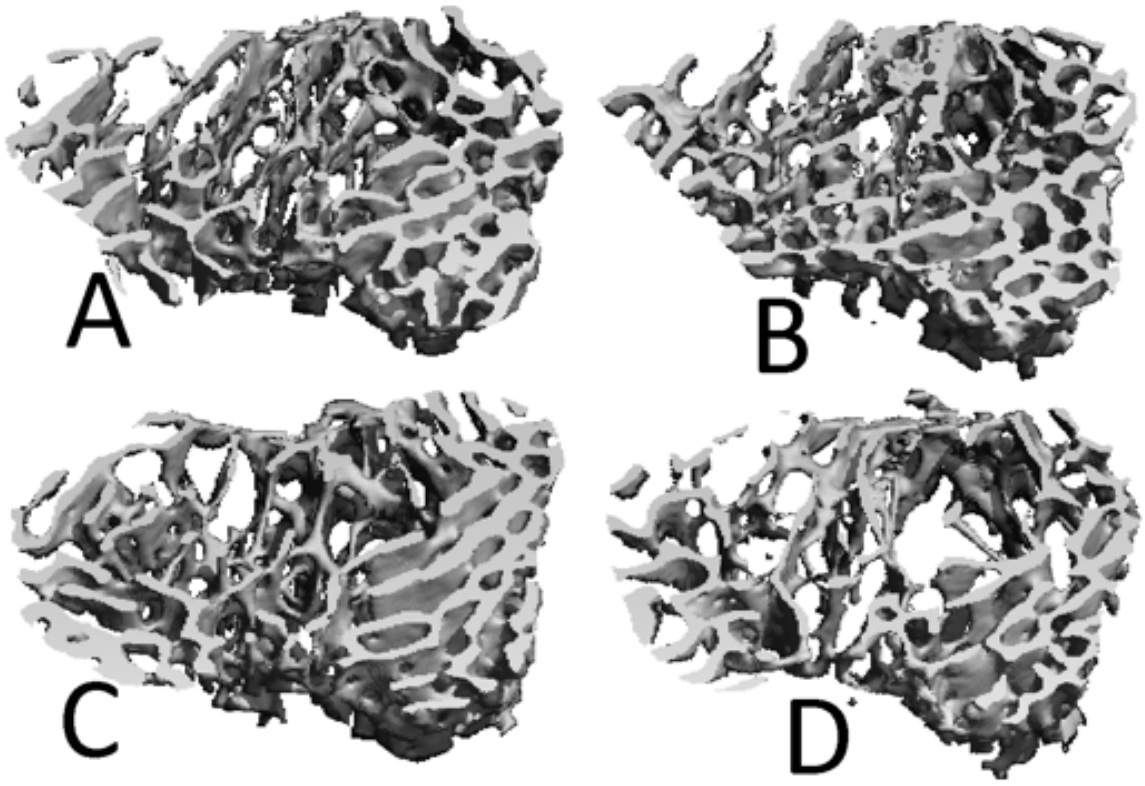

Figure 5 – Representative 3D images of trabecular bone from the proximal tibia μCT scans. A: C57 Sham; B: C57 5/6Nx; C: FVB Sham; D: FVB 5/6Nx

Quantitative analysis of both trabecular and cortical microarchitecture yielded similar results. (Table 9) From the trabecular analysis the FVB sham mice had significantly lower bone volume-to-total volume fracture (BV/TV; -38.1%), trabecular number (Tb.N; -23.8%), connectivity density (Conn.D; -48.6%), and higher trabecular spacing (Tb.Sp; +38.3%) and structural model index (SMI; +18.1%), as compared to the C57 sham mice. In 3-point bending the FVB sham mice had 26.1% lower yield strength than the C57 sham mice (Table 10), possibly due to a 22.0% lower pMOI at the FVB femur mid-diaphysis. Although, TMD at the FVB sham femur mid-diaphysis was 2.5% greater than the in the C57 sham mice. Interestingly, while femur mid-diaphysis cortical mineral density was higher in the FVB sham mice, FVB proximal tibia trabecular mineral density was actually 40.59% lower than the C57 mice among the sham groups. Compositional analysis revealed no change in percent mineral in the humerus between strains. However, the FVB sham mice possessed a 10.4% higher mean mineral mass than the C57 sham mice. (Table 11)

The cortical bone cross-sectional area data from the quantitative histomorphometry analysis of the tibia showed a significant difference between both strains in which the FVB sham mice have 8.9% less cortical bone area in the tibia shaft than the C57 sham mice. Dynamic labeling among the mice in this study was inconsistent and no significant differences were observed when comparing strains, possibly due to the mature age of the mice. Only 51.0% of all samples in the study showed any labeled periosteal bone apposition and only 54.9% showed any labeled endocortical bone apposition (23.5% showed both periosteal and endocortical bone apposition).

Table 9 – Bone microarchitecture data as measured by either µCT or quantitative histomorphometry. The trabecular data is from analysis of the proximal tibia and the cortical data is from analysis of femur mid-diaphysis. All data is presented as mean ± SD. Due to the general absence of labeled perimeter on many samples, bone formation area and rate data presented only includes samples that showed label on either the periosteal and/or the endocortical surfaces as indicated by lower number of samples per analysis.

		FVB		C57	
	Method	*Sham (n = 12)*	*5/6 Nx (n = 13)*	*Sham (n = 12)*	*5/6 Nx (n = 13)*
Trabecular Bone					
BV/TV (%)	µCT	9.53 ± 2.94	9.89 ± 2.75	15.41 ± 2.48 †	15.35 ± 1.71
vBMD (mg HA/cm^3)	µCT	89.33 ± 33.36	94.72 ± 30.06	150.37 ± 26.25 †	139.44 ± 31.01
Tb.N **	µCT	3.66 ± 0.44	3.85 ± 0.28	4.81 ± 0.28 †	4.53 ± 0.28
Tb.Sp (mm) **	µCT	0.28 ± 0.04	0.26 ± 0.02	0.20 ± 0.01 †	0.22 ± 0.01
Conn-D	µCT	64.90 ± 29.24	91.76 ± 18.83	126.32 ± 27.34 †	136.52 ± 29.57
SMI	µCT	2.04 ± 0.22	1.90 ± 0.22	1.73 ± 0.30 †	1.61 ± 0.24
Cortical Bone					
BA/TA	µCT	0.996 ± 0.004	0.996 ± 0.004	0.998 ± 0.001	0.996 ± 0.005
Bone Area (mm^2)	Q. Histo	0.681 ± 0.050	0.673 ± 0.042	0.748 ± 0.077 †	0.743 ± 0.050
Outer Perimiter (mm)	Q. Histo	3.601 ± 0.112	3.633 ± 0.079	3.979 ± 0.230 †	4.124 ± 0.184
TMD (mg HA/cm^3)	µCT	1,070.12 ± 17.05	1,049.47 ± 20.34 §	1,043.70 ± 12.36 †	1,023.98 ± 12.10 §
pMOI (mm^4)	µCT	0.33 ± 0.05	0.32 ± 0.04	0.42 ± 0.09 †	0.38 ± 0.06
Ct.Th (mm)	µCT	0.17 ± 0.01	0.15 ± 0.01 §	0.17 ± 0.01	0.16 ± 0.01
Ps.BFA (mm^2)	Q. Histo	0.0068 ± 0.0047 (n = 7)	0.0045 ± 0.0066 (n = 6)	0.0081 ± 0.0087 (n = 5)	0.0116 ± 0.0083 (n = 8)
Ps.BFR (mm^2/day)	Q. Histo	0.00048 ± 0.00033 (n = 7)	0.00032 ± 0.00047 (n = 6)	0.00058 ± 0.00062 (n = 5)	0.00083 ± 0.00060 (n = 8)
Ps.MAR (mm/day)	Q. Histo	0.00067 ± 0.00026 (n = 7)	0.00059 ± 0.00024 (n = 6)	0.00056 ± 0.00029 (n = 5)	0.00084 ± 0.00030 (n = 8)
Ec.BFA (mm^2)	Q. Histo	0.0026 ± 0.0015 (n = 6)	0.0037 ± 0.0037 (n = 7)	0.0056 ± 0.0047 (n = 9)	0.0155 ± 0.0157 (n = 6)
Ec.BFR (mm^2/day)	Q. Histo	0.00019 ± 0.00011 (n = 6)	0.00026 ± 0.00027 (n = 7)	0.00040 ± 0.00033 (n = 9)	0.00111 ± 0.00112 (n = 6)
Ec.MAR (mm/day)	Q. Histo	0.00047 ± 0.00016 (n = 6)	0.00050 ± 0.00022 (n = 7)	0.00082 ± 0.00039 (n = 9)	0.00097 ± 0.00041 (n = 6)

† $p < 0.05$ for comparison between FVB Sham and C57 Sham groups. § $p < 0.001$ for comparison between Sham and 5/6Nx groups within the strain. ** ANOVA interaction $p < 0.05$.

Table 10 - 3-pt bending of the femur and femoral neck test data presented as mean ± SD.

	FVB		C57	
	Sham	*5/6 Nx*	*Sham*	*5/6 Nx*
3 Pt Bending	*(n = 12)*	*(n = 13)*	*(n = 12)*	*(n = 14)*
Load at Yield (N)	11.88 ± 1.74	11.84 ± 2.45	16.08 ± 3.33 †	16.42 ± 2.99
Max Load (N)	18.66 ± 2.40	16.67 ± 1.70	18.46 ± 2.06	17.75 ± 2.29
Fracture Load (N)	15.51 ± 1.65	15.06 ± 1.85	15.63 ± 2.39	15.18 ± 3.68
Stiffness (N/mm)	116.42 ± 22.15	105.25 ± 16.14	112.34 ± 14.25	110.16 ± 20.36
Femoral Neck	*(n = 11)*	*(n = 11)*	*(n = 12)*	*(n = 14)*
Load at Yield (N)	16.13 ± 4.24	12.90 ± 5.30	20.06 ± 3.50	19.69 ± 3.14
Max Load (N)	19.25 ± 1.91	17.32 ± 1.56	21.46 ± 3.10	22.25 ± 2.49
Fracture Load (N)	19.00 ± 1.75	17.06 ± 1.57	18.60 ± 4.53	21.34 ± 2.61
Stiffness (N/mm)	154.08 ± 34.05	141.85 ± 26.68	165.39 ± 18.55	160.05 ± 19.89

† $p < 0.01$ for comparison between FVB sham and C57 sham groups.

Table 11 – Ashing mineral composition data. All data is presented as mean ± SD.

	FVB		C57	
	Sham (n = 12)	*5/6 Nx (n = 13)*	*Sham (n =12)*	*5/6 Nx (n = 14)*
Dry Mass (mg)	23.10 ± 1.61	23.06 ± 0.93	21.22 ± 2.31	21.74 ± 1.27
Mineral Mass (mg)	13.83 ± 0.88	13.88 ± 0.74	12.53 ± 1.27 †	12.46 ± 0.53
Percent Mineral	59.95 ± 2.09	60.16 ± 1.36	59.81 ± 9.85	57.39 ± 2.04

† $p < 0.01$ for comparison between sham groups.

6.4 Discussion

In this study we investigated bone characteristics of the FVB inbred strain of mice and compared them to an inbred strain of known low bone density, the C57 strain. Furthermore, we set out to study the effects of 5/6Nx, an established surgical method of modeling moderate kidney disease, on both strains of mice. Specifically, we wanted to quantify the effects of 5/6Nx on the bone tissue of both strains of mice from both morphological and mechanical perspectives.

The results of the trabecular μCT analysis indicate that the FVB sham mice have an even lower quality trabecular microarchitecture than the C57 sham mice. The amount of trabecular bone within the μCT scan region, as well as the number of trabeculae, the distance between them, and the bone mineral density all confirm this observation. Furthermore, non-dynamic μCT measures of Conn.D and SMI also indicate that these two strains have significantly different trabecular morphology. The FVB sham proximal tibiae showed an SMI value closer to 3 and thus have a higher ratio of cylindrical rod-like trabeculae, while the C57 sham mice have an SMI value that is closer to 0 thus indicating a higher ratio of parallel plates in the trabecular bone of the proximal tibia. The C57 sham mice also show a much higher degree of connectivity within the trabecular bone than the FVB mice, as measured in Conn.D. From a functional perspective both SMI and Conn.D indicate that the FVB mice have less robust trabecular microarchitecture, which likely equates to decreased mechanical strength in the cancellous bone.

However, genetic influences on bone quality have been shown to be compartment and site-specific. [35] Because trabecular bone has much more marrow-to-bone surface contact it is more likely to change due to metabolic influences than cortical bone. FVB

mice could therefore have poor trabecular bone microarchitecture due to a genetic disposition to higher bone turnover, but because there is less marrow contact in cortical bone, this same genetic influence could be muted in the cortical tissue. The absence of significant μCT results for the cortical bone at the femur mid-diaphysis indicates as much. Interestingly, the FVB sham mice actually have significantly more dense cortical bone at the femur mid-diaphysis. But despite this difference the C57 sham femurs performed better in mechanical testing with significantly higher yield strength than the FVB mice in 3-pt bending.

Beyond the genetic influences exerted at a metabolic level, mechanical forces may also offer an explanation for the site and compartment specific results. Turner *et al.* [35] conclude that adaptations have been made in the trabecular bone of C3H mice resulting from the strength of the cortical bone. With thicker cortices and higher mineral density [8, 9], the cortical bone in C3H mice appears to carry the majority of the mechanical load, which could result in trabecular resorption. [35] This current study has similarly shown that FVB mice possess more compromised trabecular bone quality as compared to C57 mice (already considered to be a low bone mass strain that possesses few trabeculae), while at the same time also having a higher mineral density in femoral cortical bone than in the C57 mice. Therefore, another explanation why the FVB mice show impaired trabecular microarchitecture when compared to C57 mice could be due to similar adaptations as a result of physiological loads that are primarily supported by the more dense cortical bone resulting in increased trabecular resorption. The higher yield strength found in the C57 sham mice in the 3-pt bending test must then be explained by

the bone geometry of the C57 mice such that a higher pMOI in the femur gives way to better resistance to yielding in 3-pt bending.

When compared to other literature on the genetic influence on bone quality among inbred strains of mice, it is clear that FVB mice can be considered as an inbred strain of mice with low bone quality along with C57 mice. Several studies have already set out to characterize the bone quality of multiple strains of inbred mice for research [8, 9, 34, 35], all of which include the C57 strain, but none of which include the FVB strain. The data presented in this study clearly places the FVB strain below the C57 in terms of overall bone quality. The FVB strain's efficiency in creating transgenic mice should be capitalized on in future bone research that would benefit from the study of mice predisposed to poor bone quality.

In response to 5/6Nx both strains showed significantly impaired kidney function, as measured in BUN and creatinine levels, indicative of moderate kidney disease. [19] Mean values among the rest of the serum biochemical data hint at the expected trend as a result of 5/6Nx. For example, an increase in circulating PTH would indicate the expected SHPT that should result from the disruption in mineral homeostasis caused by loss of renal function. The lack of a significant result may be explained by the timeframe under which the experiment took place. Kadokawa *et al.* [19] showed significant results among the same blood serum biochemical measurements a full 20 weeks after 5/6Nx in mice aged 5-6 weeks at the time of surgery, as opposed to the 8 weeks allowed in this current work. When comparing results, duration of the diseased state might be particularly relevant in regards to serum phosphate and PTH. Perhaps 8 weeks following 5/6Nx is too soon to see the pronounced mineral dysregulation expected. Of specific interest in

Kadokawa's study are the measurements of circulating PTH. Kadokawa reported more than 30 fold increase in circulating PTH 20 weeks after 5/6Nx. The resultant severe SHPT is believed to be a primary player in the mineral dysregulation that eventually leads to the metabolic bone disorder associated with CKD. [12] One other relevant difference between Kadokaw's study and this current work is the high phosphate diet given to the mice in Kadokawa's study whereas our mice were provided with a normal phosphate diet. The increased dietary phosphate load exasperated the mineral homeostasis and drove PTH levels further upward, which in addition to the influence of decreased renal function, caused the severe increase in PTH levels. In this current study the mice were fed a normal chow diet, and therefore did not respond with as severe of an increase in PTH circulation.

While the length of the disease course in this current study was not long enough to elicit a significant trabecular response, cortical tissue did show some response. Both strains were affected by 5/6Nx showing a decrease in mineral density and cortical thickness at the femur mid-diaphysis (note that cortical thickness in the C57 strain was not significantly altered). Neither the mineral density nor cortical thickness changes due to 5/6Nx had an effect on the mechanical properties however, as no significant changes were observed in the mechanical data. It appears therefore that the FVB cortical bone was the first skeletal region of interest to show the effects of metabolic bone disorder due to 5/6Nx. It seems reasonable, based on the full set of data, to conclude that cortical bone is affected first in this model with trabecular bone changes appearing somewhere between 8 weeks and 20 weeks post surgery. By administering a high phosphate diet, it is also

possible to exasperate the mineral disequilibrium and accelerate the bone changes due to 5/6Nx.

In the C57 mice, both RANKL and OPG expression increased as a result of 5/6Nx, while in the FVB mice, expression of both decreased. Although gene expression among both strains changed minimally as a result of 5/6Nx. RANKL and OPG are competitive antagonists both binding to RANK which activates osteoclasts when it is bound to RANKL. [30, 31, 37] Therefore the ratio between RANKL and OPG should give a picture of the state of osteoclasts within the bone tissue. In the C57 mice OPG expression increased at a greater rate than RANKL as a result of 5/6Nx, which would lead to an OPG heavier influence in osteoclastic activity, or less osteoclast activation. While in the FVB mice both genes decreased in expression but with RANKL expression decreasing to a lesser extent than OPG expression. Therefore the FVB mice appear to have a heavier RANKL ratio within the bone and would therefore possess higher osteoclast activation, and higher rates of bone turnover. While this is certainly not the whole picture of what is happening on a genetic level, it does hint at some of the changes that take place in mice with CKD in regards to the molecular players involved in bone metabolism.

By including the FVB strain in the study we have been able to broaden future research horizons for bone research using murine models. Successfully characterizing FVB bone quality from both morphological and mechanical perspectives and placing it into context among other commonly used inbred strains of mice should set the stage for using this strain in a variety of bone research. Specifically in regards to CKD research, we have also provided a basis for understanding the effects of 5/6Nx as a model of

moderate kidney disease and indicated that a longer disease course is likely necessary for the full systemic effects of renal failure to be seen in bone tissue and mineral metabolism. Chronic kidney disease involves multiple organ systems and its effects across the entire body are complex. As therapy for CKD improves on other fronts, the importance of understanding the effects of the disease on bone tissue becomes more critical from a clinical perspective while research models utilizing inbred mice and different surgical methods of simulating CKD will pave the way for the development of clinical therapies in the future.

7. Discussion and Conclusions

The primary objective of these studies was to explore and quantify the bone effects that result from CKD. This work was undertaken through murine models with a focus on the structure-function relationship within their bone and the response to loss of renal function. Two different surgical methods of replicating the effects of CKD were chosen to model varying degrees of kidney dysfunction: UNx to model mild CKD and 5/6Nx to model moderate to severe CKD. Furthermore, the dietary phosphate binding compound sevelamer was also studied to determine the role of the dietary phosphate load on mineral homeostasis in a state of kidney dysfunction. Additionally, we provided a complete characterization of the bone quality of a previously uncharacterized strain of inbred mice, FVB, to be added to the repertoire of murine models used for bone research.

In general, surgically induced CKD was accompanied with a decrease in bone quality as measured in μCT morphological analysis, mechanical testing, and quantitative histomorphometry. The degree of these changes, however, were not the broad, clear bone changes that we anticipated. This is likely due to the fact that the bone-kidney axis [38] that is disrupted during CKD is complex and the pathogenesis of CKD-MBD that results can vary from individual to individual. So instead of seeing bone changes across all morphological and mechanical measures, we only saw significant changes in a couple of outcomes as a result of either UNx or 5/6Nx. With UNx the resulting CKD did not yield any statistically significant changes due to loss of renal function. Several trabecular outcomes, however, did show a trend towards the expected changes. This is likely due to the fact that UNx models mild CKD and the bone effects were not severe because the mice were able to maintain a relatively normal mineral homeostasis despite loss of one

kidney. In the case of the 5/6Nx FVB mice some cortical changes did occur as a result of the surgery, however, those changes were not manifested in the mechanical properties of the cortical bone. In this case the absence of bone changes was due to the both the duration of the disease in the mice and the diet they were fed. It appears now that in order to elicit broad, clear bone changes in mice one must both let the disease run a longer course and help the mineral disequilibrium along by the inclusion of a high phosphate diet as in Kadokawa *et al.* [19]

Across all of the data presented in this thesis, we also universally observed a large degree of variability between samples within the same experimental groups. Statistically significant results were difficult to obtain because of high standard deviations within groups. This might be due to the complicated, systemic nature of this disease and that it might be even more unpredictable in mice. Increasing the number of samples in the study would help mitigate those high standard deviations. Looking at the data qualitatively, and on a sample-to-sample basis, however, it was clear that both surgical models did have an effect on the bone of some individual mice. Yet there were still enough samples in the studies that showed less response, or none at all, to drive standard deviations up.

Ultimately, the hypotheses that we set out to test were examined effectively and we were able to learn about the effects of CKD on the bone of mice. In the pathogenesis of CKD-MBD we now know that bone changes do not occur quickly and uniformly, but sometimes slowly and erratically in mice. What changes were noticed indicated that bone morphology and mechanical properties generally deteriorate as a result of loss of renal function. Furthermore, a successful characterization of the bone quality of the FVB inbred strain of mice should also now make that strain available as an option for

conducting bone research, particularly in cases where an inbred strain of low bone quality is needed in studies requiring transgenic samples.

8. References

[1] A. S. Levey and J. Coresh, "Chronic kidney disease," *The Lancet*, vol. 379, no. 9811, pp. 165–180, Jan. 2012.

[2] T. L. Nickolas, M. B. Leonard, and E. Shane, "Chronic kidney disease and bone fracture: a growing concern," *Kidney International*, vol. 74, no. 6, pp. 721–731, Sep. 2008.

[3] C. P. Kovesdy and K. Kalantar-Zadeh, "Bone and mineral disorders in pre-dialysis CKD," *Int Urol Nephrol*, vol. 40, no. 2, pp. 427–440, Jun. 2008.

[4] O. Gutierrez, "Fibroblast Growth Factor-23 Mitigates Hyperphosphatemia but Accentuates Calcitriol Deficiency in Chronic Kidney Disease," *Journal of the American Society of Nephrology*, vol. 16, no. 7, pp. 2205–2215, Apr. 2005.

[5] N. S. Bricker, "On the pathogenesis of the uremic state. An exposition of the 'trade-off hypothesis'," *The New England Journal of Medicine*, vol. 286, no. 20, pp. 1093–1099, May 1972.

[6] K. A. Hruska, S. Mathew, R. Lund, P. Qiu, and R. Pratt, "Hyperphosphatemia of chronic kidney disease," *Kidney International*, vol. 74, pp. 148–157, Apr. 2008.

[7] R. F. Klein, "J Musculoskelet Neuronal Interact 2008 Klein," *J Musculoskeletal Neuronal Interact*, pp. 1–4, Jan. 2009.

[8] W. Beamer, L. Donahue, C. Rosen, and D. J. Baylink, "Genetic Variability in Adult Bone Density Among Inbred Strains of Mice," *Bone*, pp. 1–7, Mar. 2003.

[9] M. P. Akhter, U. T. Iwaniec, M. A. Covey, D. M. Cullen, D. B. Kimmel, and R. R. Recker, "Genetic Variations in Bone Density, Histomorphometry, and Strength in Mice," *Calcified Tissue International*, vol. 67, no. 4, pp. 337–344, Oct. 2000.

[10] V. L. Ferguson, R. A. Ayers, T. A. Bateman, and S. S. J, "Bone development and age-related bone loss in mal C57BL/6J mice," *Bone*, pp. 387–398, Sep. 2003.

[11] B. P. Halloran, V. L. Ferguson, S. S. J, A. Burghardt, L. L. Venton, and S. Majumdar, "Changes in Bone Structure and Mass With Advancing Age in the Male C57BL/6J Mouse," *Journal of Bone and Mineral Research*, vol. 17, no. 6, pp. 1044–1050, Apr. 2002.

[12] K. J. Martin and E. A. Gonzalez, "Metabolic Bone Disease in Chronic Kidney Disease," *Journal of the American Society of Nephrology*, vol. 18, no. 3, pp. 875–885, Jan. 2007.

[13] K. Kiattisunthorn and S. M. Moe, "Chronic kidney disease-mineral bone disorder (CKD-MBD)," *IBMS BoneKEy*, vol. 7, no. 12, pp. 447–457, Dec. 2010.

[14] M. M. Lee, E. Y. Chu, M. M. El-Abbadi, B. L. Foster, K. A. Tompkins, C. M. Giachelli, and M. J. Somerman, "Characterization of mandibular bone in a mouse model of chronic kidney disease," *Journal of Periodontology*, vol. 81, no. 2, pp. 300–309, Aug. 2009.

[15] T. L. Nickolas, D. J. McMahon, and E. Shane, "Relationship between Moderate to Severe Kidney Disease and Hip Fracture in the United States," *Journal of the American Society of Nephrology*, vol. 17, no. 11, pp. 3223–3232, Sep. 2006.

[16] A. C. Dooley, N. S. Weiss, and B. Kestenbaum, "Increased Risk of Hip Fracture Among Men With CKD," *American Journal of Kidney Diseases*, vol. 51, no. 1, pp. 38–44, Jan. 2008.

[17] A. Mittalhenkle, D. L. Gillen, and C. O. Stehman-Breen, "Increased risk of mortality associated with hip fracture in the dialysis population," *American Journal of Kidney Diseases*, vol. 44, no. 4, pp. 672–679, Oct. 2004.
[18] R. J. Lund, "Successful Treatment of an Adynamic Bone Disorder with Bone Morphogenetic Protein-7 in a Renal Ablation Model," *Journal of the American Society of Nephrology*, vol. 15, no. 2, pp. 359–369, Feb. 2004.
[19] S. Kadokawa, T. Matsumoto, H. Naito, and M. Tanaka, "Assessment of Trabecular Bone Architecture and Intrinsic Properties of Cortical bone Tissue in a Mouse Model of Chronic Kidney Disease," *Journal of Hard Tissue Biology*, vol. 20, no. 2, pp. 79–86, Jun. 2011.
[20] M. L. Bouxsein, S. K. Boyd, B. A. Christiansen, R. E. Guldberg, K. J. Jepsen, and R. Müller, "Guidelines for assessment of bone microstructure in rodents using micro-computed tomography," *Journal of Bone and Mineral Research*, vol. 25, no. 7, pp. 1468–1486, Jun. 2010.
[21] P. Rüegsegger, B. Koller, and R. Müller, "A Microtomographic System for the Nondestructive Evaluation of Bone Architecture," *Calcified Tissue International*, vol. 58, pp. 24–29, Oct. 1996.
[22] J. Bonadio, T. L. Saunders, E. Tsai, S. A. Goldstein, J. Morris-Wiman, L. Brinkley, D. F. Dolan, R. A. Altschuler, J. E. Hawkins, J. F. Bateman, T. Mascara, and R. Jaenisch, "Transgenic mouse model of the mild dominant form of osteogenesis imperfecta," *Proceedings of the National Academy of Sciences of the United States of America*, vol. 87, pp. 7145–7149, Sep. 1990.
[23] L. B. Engesaeter, A. Ekeland, and N. Langeland, "Methods for Testing the Mechanical Properties of the Rat Femur," *Acta Orthopaedica Scandinavica*, vol. 49, no. 6, pp. 512–518, Aug. 1978.
[24] T. Jämsä, J. Tuukkanen, and P. Jalovaara, "Femoral neck strength of mouse in two loading configurations: method evaluation and fracture characteristics," *Journal of Biomechanics*, vol. 31, pp. 723–729, Sep. 1998.
[25] C. H. Turner, Y. Takano, and T. Hirano, "Reductions in Bone Strength After Fluoride Treatment Are Not Reflected in Tissue-Level Acoustic Measurements," *Bone*, vol. 19, no. 6, pp. 603–607, Mar. 1996.
[26] M. D. Brodt, C. B. Ellis, and M. J. Silva, "Growing C57Bl/6 Mice Increase Whole Bone Mechanical Properties by Increasing Geometric and Material Properties," *Journal of Bone and Mineral Research*, vol. 14, no. 12, pp. 2159–2166, Nov. 1999.
[27] V. L. Ferguson, "Age-related bone loss and treatment with cytokines in mice," University of Colorado, 2001.
[28] T. C. Sun, S. Mori, J. Roper, C. Brown, T. Hooser, and D. B. Burr, "Do Different Fluorochrome Labels Give Equivalent Histomorphometric Information?T.C.," *Bone*, vol. 13, pp. 443–446, Jul. 1992.
[29] K. R. Gordon, P. Burns, and G. Keller, "Experimental Changes in Mineral Content of Juvenile Mouse Femora," *Calcified Tissue International*, vol. 51, pp. 229–232, Oct. 1991.
[30] L. J. Raggatt and N. C. Partridge, "Cellular and Molecular Mechanisms of Bone Remodeling," *Journal of Biological Chemistry*, vol. 285, no. 33, pp. 25103–25108, Aug. 2010.

[31] N. Nakagawa, M. Kinosaki, K. Yamaguchi, N. Shima, H. Yasuda, K. Yano, T. Morinaga, and K. Higashio, "RANK Is the Essential Signaling Receptor for Osteoclast Differentiation Factor in Osteoclastogenesis," *Biochemical and Biophysical Research Communications*, vol. 253, no. 2, pp. 395–400, Dec. 1998.

[32] Y. Iwasaki, J. J. Kazama, H. Yamato, and M. Fukagawa, "Changes in chemical composition of cortical bone associated with bone fragility in rat model with chronic kidney disease," *Bone*, vol. 48, no. 6, pp. 1260–1267, Jun. 2011.

[33] J. Bacchetta, S. Boutroy, N. Vilayphiou, L. Juillard, F. Guebre-Egziabher, N. Rognant, E. Sornay-Rendu, P. Szulc, M. Laville, P. D. Delmas, D. Fouque, and R. Chapurlat, "Early Impairment of Trabecular Microarchitecture Assessed With HR-pQCT in Patients With Stage II-IV Chronic Kidney Disease," *Journal of Bone and Mineral Research*, pp. 090923081446048–090923081446024, Sep. 2009.

[34] I. Sabsovich, J. D. Clark, G. Liao, G. Peltz, D. P. Lindsey, C. R. Jacobs, W. Yao, T.-Z. Guo, and W. S. Kingery, "Bone microstructure and its associate genetic variability in 12 inbred mouse strains: uCT study and in silico genome scan," *Bone*, vol. 42, pp. 439–451, Sep. 2007.

[35] C. H. Turner, Y.-F. Hsieh, R. Müller, M. L. Bouxsein, D. J. Baylink, C. J. Rosen, M. D. Grynpas, L. R. Donahue, and W. G. Beamer, "Genetic Regulation of Cortical and Trabecular Bone Strength and Microstructure in Inbred Strains of Mice," *Journal of Bone and Mineral Research*, vol. 15, no. 6, pp. 1126–1131, May 2000.

[36] M. Taketo, A. C. Schroeder, L. E. Mobraaten, K. B. Gunning, G. Hanten, R. R. Fox, T. H. Roderick, C. L. Stewart, F. Lilly, C. T. Hansen, and P. A. Overbeek, "An inbred mouse strain preferable for transgenic analyses," *Proceedings of the National Academy of Sciences of the United States of America*, vol. 88, pp. 2065–2069, Apr. 2013.

[37] H. Yasuda, N. Shima, N. Nakagawa, K. Yamaguchi, M. Kinosaki, M. Goto, S. I. Mochizuki, E. Tsuda, T. Morinaga, N. Udagawa, N. Takahasi, T. Suda, and K. Higashio, "A Novel Molecular Mechanism Modulating Osteoclast Differentiation and Function," *Bone*, vol. 25, no. 1, pp. 109–113, Jun. 1999.

[38] J. Danziger, "The bone-renal axis in early chronic kidney disease: an emerging paradigm," *Nephrology Dialysis Transplantation*, vol. 23, no. 9, pp. 2733–2737, Apr. 2008.